



High-Performance Al–Si Coatings Toward Enhancing Oxidation Resistance of Tungsten by Halide-Activated Pack Cementation

Liu Zhu¹, Yu-Xiang Zhang², Jin-Fang Wang¹ and Lai-Ma Luo^{2*}

¹ School of Pharmaceutical and Materials Engineering, Taizhou University, Taizhou, China, ² School of Materials Science and Engineering, Hefei University of Technology, Hefei, China

An aluminide–silicide coating was prepared on a pure tungsten substrate by halide-activated pack cementation. Thickness, morphology, and phase structure of the Al–Si coating were systematically investigated. Thermal cyclic oxidation tests of the Al–Si coating were carried out at 1,000°C. The results revealed that the aluminide and silicide coating possessed relatively high cyclic oxidation resistance against high temperature. After oxidation, dense SiO₂ and Al₂O₃ were formed in the coating. Oxidation rate of the Al–Si coating was lower than that of the pure tungsten.

OPEN ACCESS

Edited by:

Hongwei Shi,
Institute of Metals Research (CAS),
China

Reviewed by:

Jian Chen,
University of Western Ontario, Canada
Inime Ime Udoh,
Shenyang Ligong University, China

*Correspondence:

Lai-Ma Luo
luolaima@126.com

Specialty section:

This article was submitted to
Environmental Materials,
a section of the journal
Frontiers in Materials

Received: 14 January 2020

Accepted: 21 April 2020

Published: 04 June 2020

Citation:

Zhu L, Zhang Y-X, Wang J-F and
Luo L-M (2020) High-Performance
Al–Si Coatings Toward Enhancing
Oxidation Resistance of Tungsten by
Halide-Activated Pack Cementation.
Front. Mater. 7:136.
doi: 10.3389/fmats.2020.00136

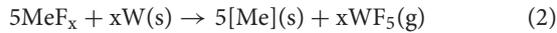
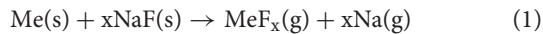
Keywords: Al–Si coating, tungsten, oxidation protection, pack cementation, 316L stainless steel matrix

INTRODUCTION

Tungsten has been considered as a promising high-temperature and irradiation-resistant material in nuclear energy industry applications owing to its high melting point, high-temperature stability, and other advantages (Wang et al., 2014; Tan et al., 2019). However, unsatisfactory durability of tungsten materials against high-temperature oxidation limits their applications (Cai et al., 2018; Liu D. G. et al., 2018). So far, various approaches have been developed in improving oxidation resistance of refractory metals (Wang et al., 2017; Bobzin et al., 2018). Among them, it has been proven one of the most effective solutions to constructing aluminide and silicide coatings on the tungsten substrate, such as Al₄W and WSi₂, which can reduce the high-temperature oxidation rate because of coating adherence, thermal expansion, and cost efficiency (Pei et al., 2017; Wu et al., 2018).

Usually physical vapor deposition (Pulci et al., 2015; Swadzba, 2018), metal organic chemical vapor deposition (M'Saoubi et al., 2017), hot dipping (HD) (Oukati et al., 2018; Zhang et al., 2018), and halide-activated pack cementation (HAPC) (Majumdar et al., 2017) are used to prepare aluminide and silicide layers. However, some problems have to be dealt with for these methods. Physical vapor deposition is not a suitable technique to prepare dense and uniform coating; coatings prepared by hot dip aluminizing are prone to void; electrochemical deposition is suitable for the deposition on the substrate with complex shape and exhibits stable performance, but the technology requires high temperature (Sun et al., 2017). In terms of HAPC, it has attracted more and more interest in preparing aluminum and silicon diffusion layer (Tian et al., 2014; Qiao et al., 2018). Halide-activated pack cementation processes are relatively cheap and cost-effective (Bozza et al., 2014). During the process, a substrate is packed in filler agent based on a metal powder, which acts as a metal source and an activator. By reacting with the metal source to form gas phase, the steam containing metal phase is transported to component surface and inert filler to restrain the sintering and agglomeration of the metal powder. During the pack cementation process, it is believed that

the active Si and Al are formed based on the following chemical reactions (Cheng et al., 2015; Liu Y. et al., 2018):



where Me is Si ($x = 1-4$) or Al ($x = 1-3$) in this study.

In this process, the generated silicide and aluminum coatings improve the oxidation resistance of the substrate by forming a compact and uniform antioxidation coating in a high-temperature environment, which prevents the bare substrate from destructive oxidation. In addition, the coatings feature cost-effectiveness and self-healing characteristics (Wang L. et al., 2018; Wu et al., 2019).

In this article, four coating systems were codeposited on the surface of the pure tungsten substrate. Scanning electron microscope (SEM), energy-dispersive X-ray spectroscopy (EDS), X-ray diffractometer (XRD), and X-ray photoelectron spectroscopy (XPS) were used to characterize thickness, morphology, chemical composition, and phase structure of the Al-Si coatings. The oxidation protection performance of coated and uncoated tungsten samples was evaluated by thermal cycling oxidation test at 1,000°C.

EXPERIMENTAL DETAILS

Specimen Preparation

In this article, pure tungsten (the W content $\geq 99.95\%$) was selected as the substrate for research. Samples were cut with an electrical machine to obtain several $10 \times 10 \times 2$ -mm samples for subsequent experiments. The samples used for packing cementation were well mechanically polished until mirror-like

surface and then clean it in acetone bath for 20 min and dry it completely.

Coating Process

In the course of pack cementation process, the samples were buried in sealed crucibles with powder mixture. **Table 1** shows the chemical composition of the corresponding powder mixture. As for the powder mixture, NaF acts as activator and Al_2O_3 as inert filler to avoid Al and Si sintering in the course of aluminizing and silicide process. The powders were uniformly mixed in a planetary ball mill for 4 h, and then the mixed powder was poured into a covered alumina crucible. Further, the sample was buried in the mixed powder and sealed with a silica sol. Aluminizing and siliconizing processes of samples were executed at 1,000°C for 5 h with argon. After aluminizing and siliconizing, the specimens were ultrasonically cleaned in acetone and dried. The method can easily obtain a uniform and dense coating.

Figure 1 shows the formation mechanism of the aluminized and siliconized coating. Aluminum and silicon atoms react with the activator under high temperature to form active aluminum and silicon atoms. Active atoms first absorb onto the surface of the substrate and dissolve into the tungsten to form a solid solution. When the aluminum atoms increase to a certain quantity, the tungsten-aluminum and tungsten-silicon alloy layer begins to form. Aluminum, silicon, and tungsten atoms diffuse each other, and the aluminized and siliconized layers gradually thicken (Sun et al., 2017).

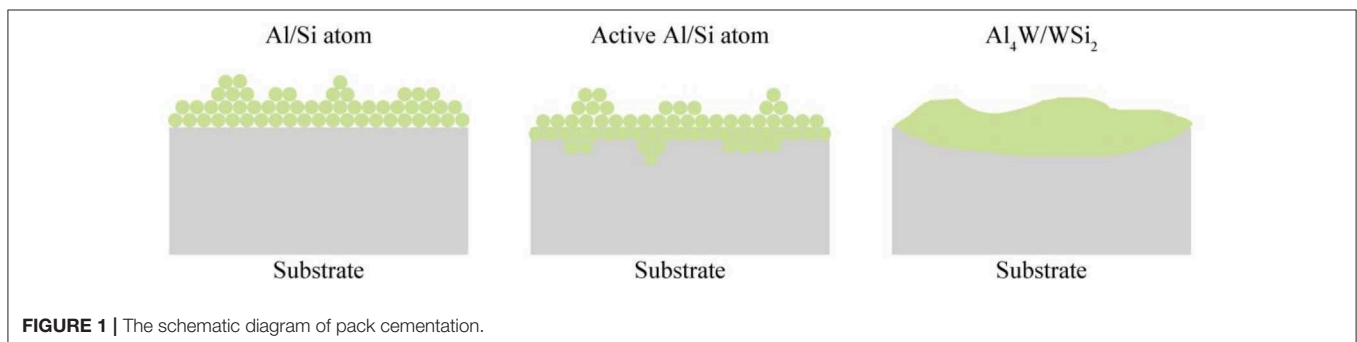
Analytical Methods

The surface morphology and thickness of the coating were analyzed by FE-SEM (SU8020). X-ray diffractometer and XPS were used to analyze the crystal phase of the coating. X-ray uses $\text{Cu-K}\alpha$ for radiation, the wavelength is 0.1540598 nm, the voltage is 40 kV, the current is 40 mA, the diffraction angle ranges from 10 to 90°, and the incoming angle is 2.5°. Surface roughness values of the coating were evaluated by a surface profiler.

Cyclic oxidation tests were performed on coated and uncoated samples in a tube furnace at 1,000°C in air. One oxidation cycle was 1 h, and the heating and cooling phases were performed in an argon atmosphere to protect the substrate. An electronic balance was used to measure the mass change of the sample in the oxidation experiment with an accuracy of 10^{-5} g. The 10- and 15-h oxidation samples were embedded in the resin to observe the evolution of the coating cross

TABLE 1 | Chemical compositions of powder mixture (in wt. %).

Sample nr.	Al	Si	NaF	Al_2O_3
S1	30	0	3	67
S2	20	10	3	67
S3	10	20	3	67
S4	0	30	3	67



section. The field emission SEM equipped with EDS was used to characterize the microstructure of the samples. The EDS was used to detect and measure the element distribution in

the sample, and the quantitative analysis accuracy of related elements was better than $\pm 1\%$. For cross-sectional investigation, the samples were embedded in resin, ground, and finally

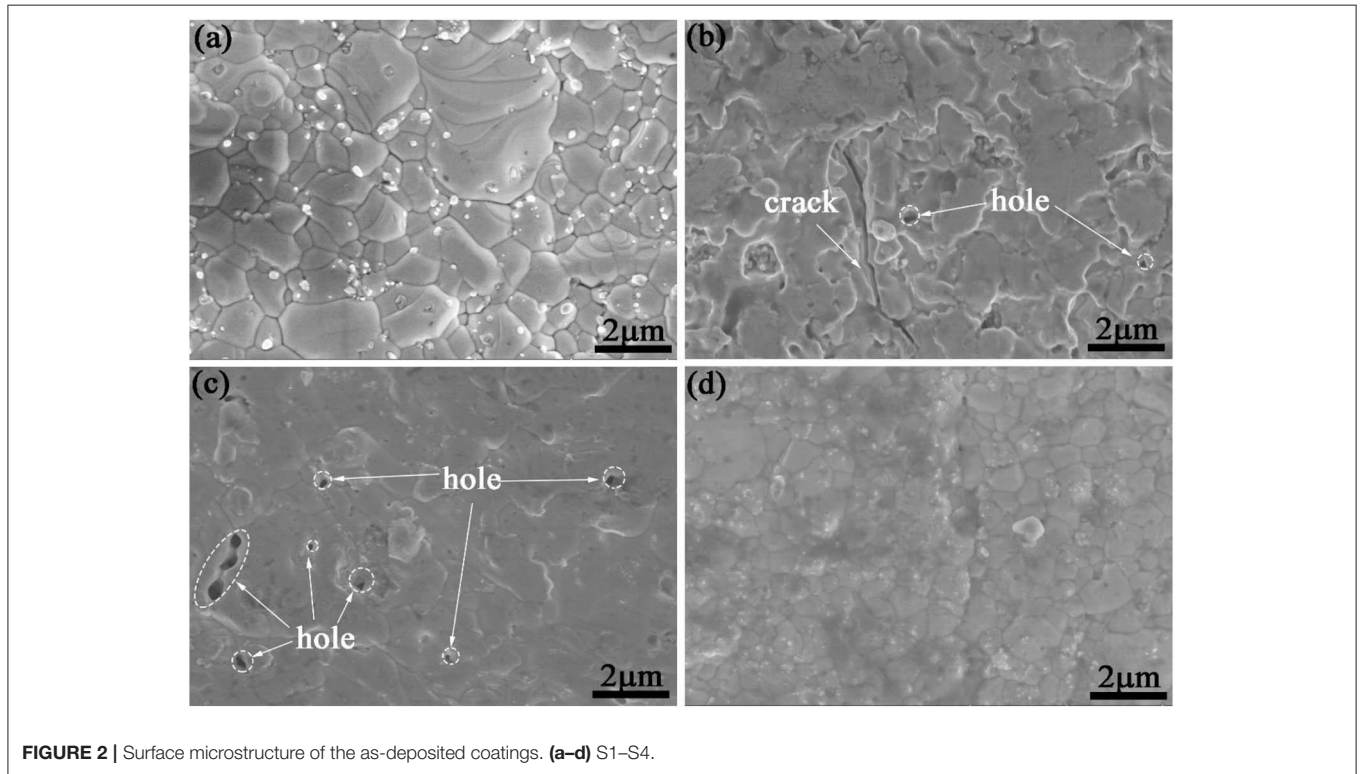


FIGURE 2 | Surface microstructure of the as-deposited coatings. (a-d) S1-S4.

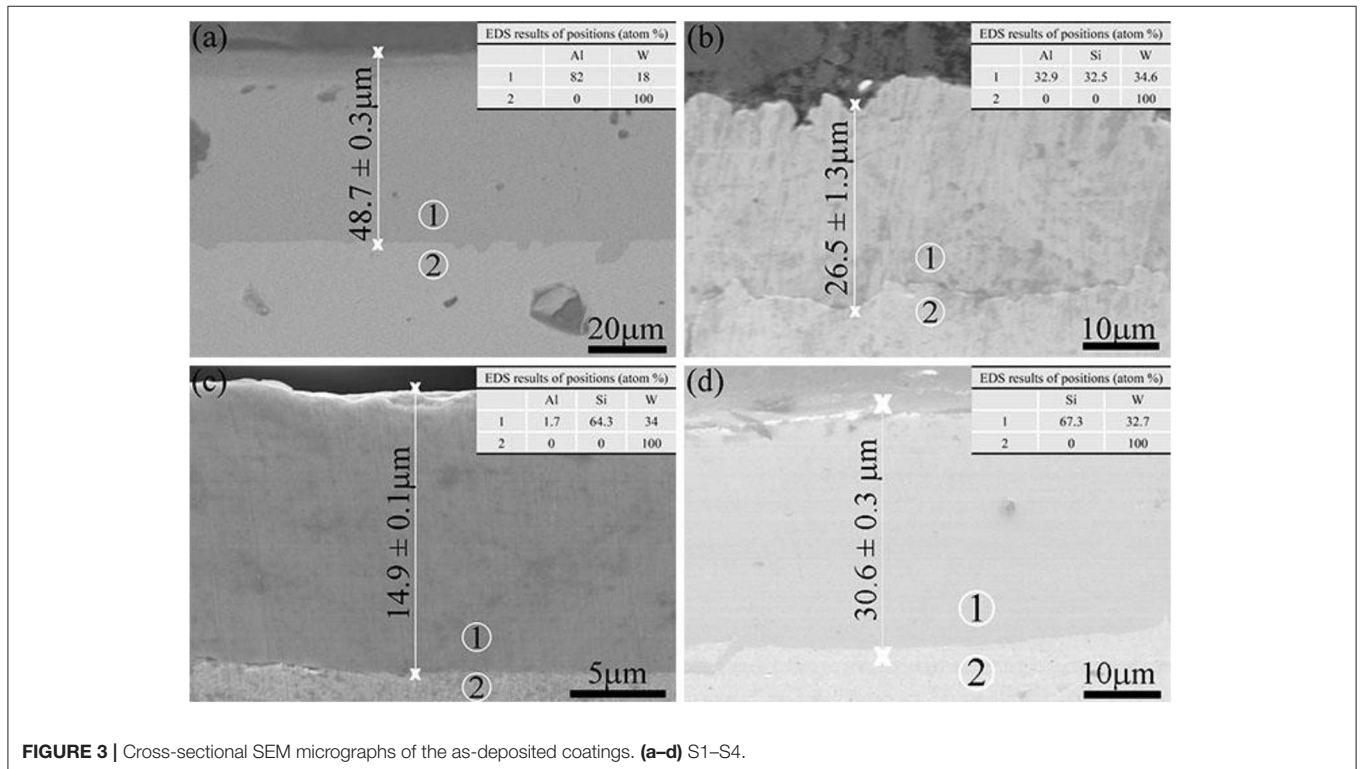


FIGURE 3 | Cross-sectional SEM micrographs of the as-deposited coatings. (a-d) S1-S4.

polished. The phases of the coatings were analyzed by XRD and XPS.

RESULTS AND DISCUSSION

Microstructure and Phase Constituents of Al-Si Coating

Scanning electron microscope images in **Figure 2** show surface morphology of the as-deposited Al and Si coating by HAPC. The coating is very continuous without obvious defects, which is further confirmed proven by the low surface roughness value measured by surface profilometer. The coating S1 with the highest Al content and the coating S4 with the highest Si content display a dense microstructure without visible cracks, as shown in **Figures 2A,D**. However, holes and cracks coating S2 and S3 are observed in **Figures 2B,C**, which commonly exist on the pack-cemented, heat-treated aluminide coating due to high manufacturing temperature and cooling procedure (Portebois et al., 2014). As for S2 and S3, the formation of holes on the surface is likely due to the following factor: insufficient heating temperature and time for packing, as well as the inadequacy of chosen activators in codepositing Al-Si metal elements (Qiao and Zhou, 2013).

FE-SEM was employed to characterize the thickness and morphology of the coating after pack cementation, and the deposition rate of the coating was determined by the ratio of the coating thickness to the processing time. In this experiment, the treatment time for all coating samples was 5 h; therefore, the deposition rate of the coatings was calculated to be 9.74,

5.30, 2.98, and 6.12 $\mu\text{m/h}$, respectively. It should be noted that there is no obvious correlation between deposition rate and chemical composition. In addition, there are no voids and second phase inclusions on the interface between the substrate and the coating as shown in **Figure 3**, which indicates a great cohesion of the sample.

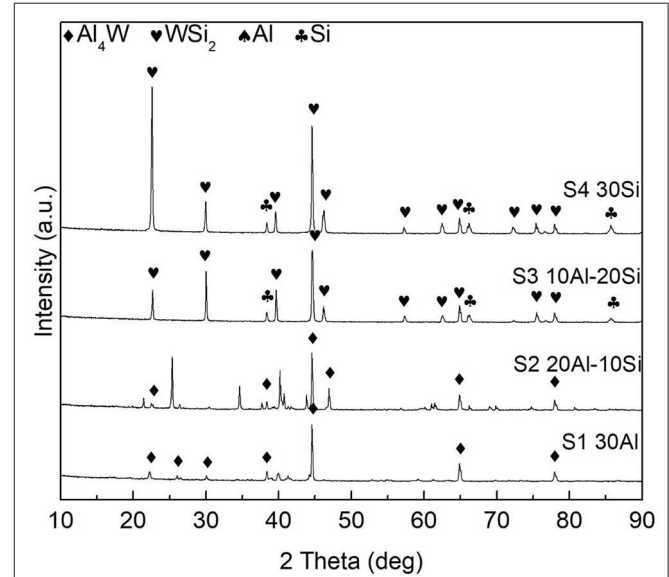


FIGURE 5 | X-ray diffractometer diffraction patterns of the as-deposited coatings S1-S4.

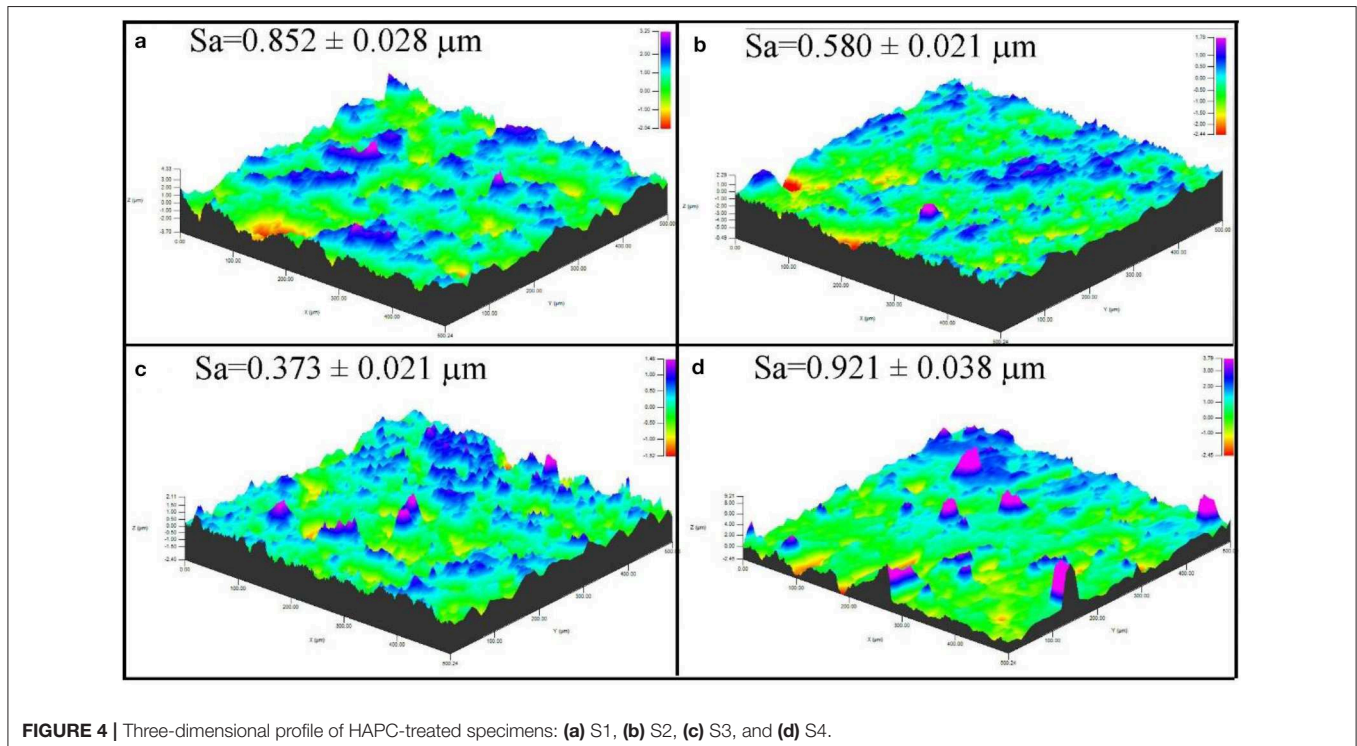


FIGURE 4 | Three-dimensional profile of HAPC-treated specimens: (a) S1, (b) S2, (c) S3, and (d) S4.

Figure 4 shows the three-dimensional (3D) profile and surface roughness value of the coating, respectively. The roughness is characterized by roughness space arithmetic mean height (RSa), which shows the variation of the surface structure. The surface of the coating S1 and S4 is relatively rough, whereas that of the coating S2 and S3 is compact and flat. Roughness space arithmetic mean height was reduced from 0.852 to 0.580 μm after reduction of Al content and the addition of Si content. When the content

of Al was reduced to 10 wt. %, the surface roughness RSa was further reduced to 0.373 μm , and the flattest and densest coating surface was achieved. Al is easy to melt in high temperature, which will cause adhesion on the surface of the substrate and then increase the surface roughness. When the Al content was continually reduced to 0%, the surface roughness RSa increased to 0.921 μm (Sun et al., 2016). Therefore, the surface is dense and consistent in morphology, as assessed by surface profilometer.

X-ray diffractometer patterns of the as-deposited coating S1 to S4 are displayed in **Figure 5**. In the coating S1 and S2, intermetallic phases Al_4W (JCPDS no. 03-065-1241) were generated. High Al activity was sustained throughout the aluminizing process, and continuous inward diffusion of Al resulted in interior layer formation within the coating. In coatings S3 and S4, intermetallic phases WSi_2 (JCPDS no. 01-081-2168) were formed. The formation process of Al_4W and WSi_2 was discussed in a previous study (Ge et al., 2018).

Thermal Cyclic Oxidation Test

Thermal Cyclic Oxidation Kinetics

Figure 6 illustrates mass change of the coated and uncoated samples during the cyclic oxidation, and the macroscopic morphology of the samples after oxidation is also shown in **Figure 7**. As shown in **Figure 6**, mass gains of aluminide and silicide coatings after a 15-h cyclic oxidation test were 41.50 and 45.96 mg/cm^2 , respectively, which were lower than those of the uncoated samples. As displayed in **Figure 7**, the coated sample was able to maintain superior integrity after the 15-h cyclic oxidation. It suggests that the coating improved the oxidation resistance of the substrate effectively.

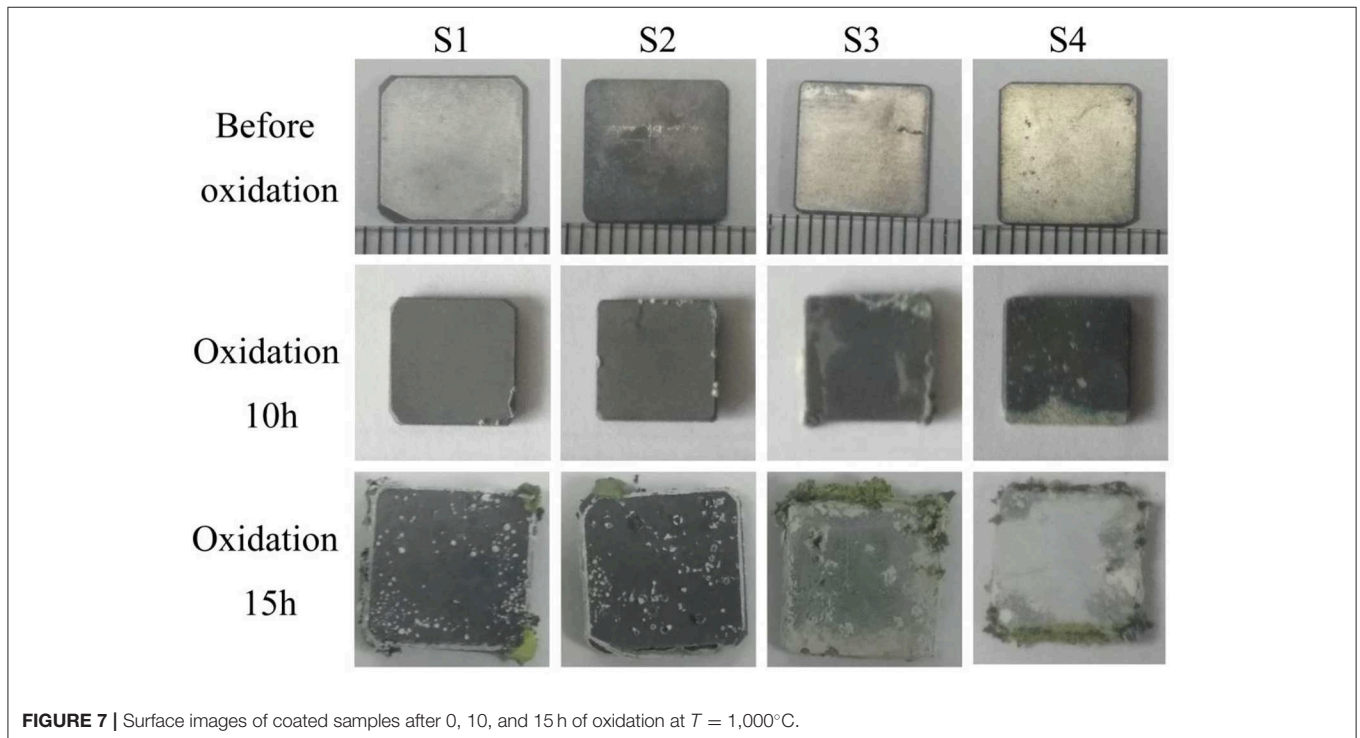
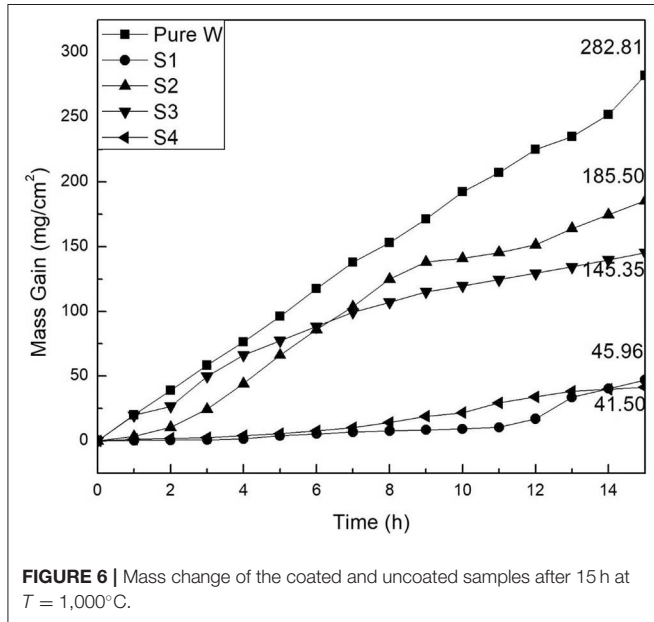
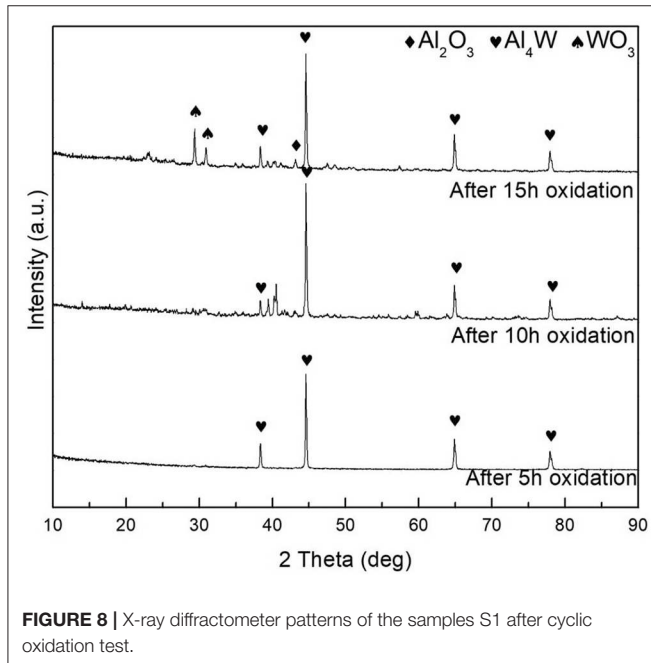


FIGURE 7 | Surface images of coated samples after 0, 10, and 15 h of oxidation at $T = 1,000^\circ\text{C}$.

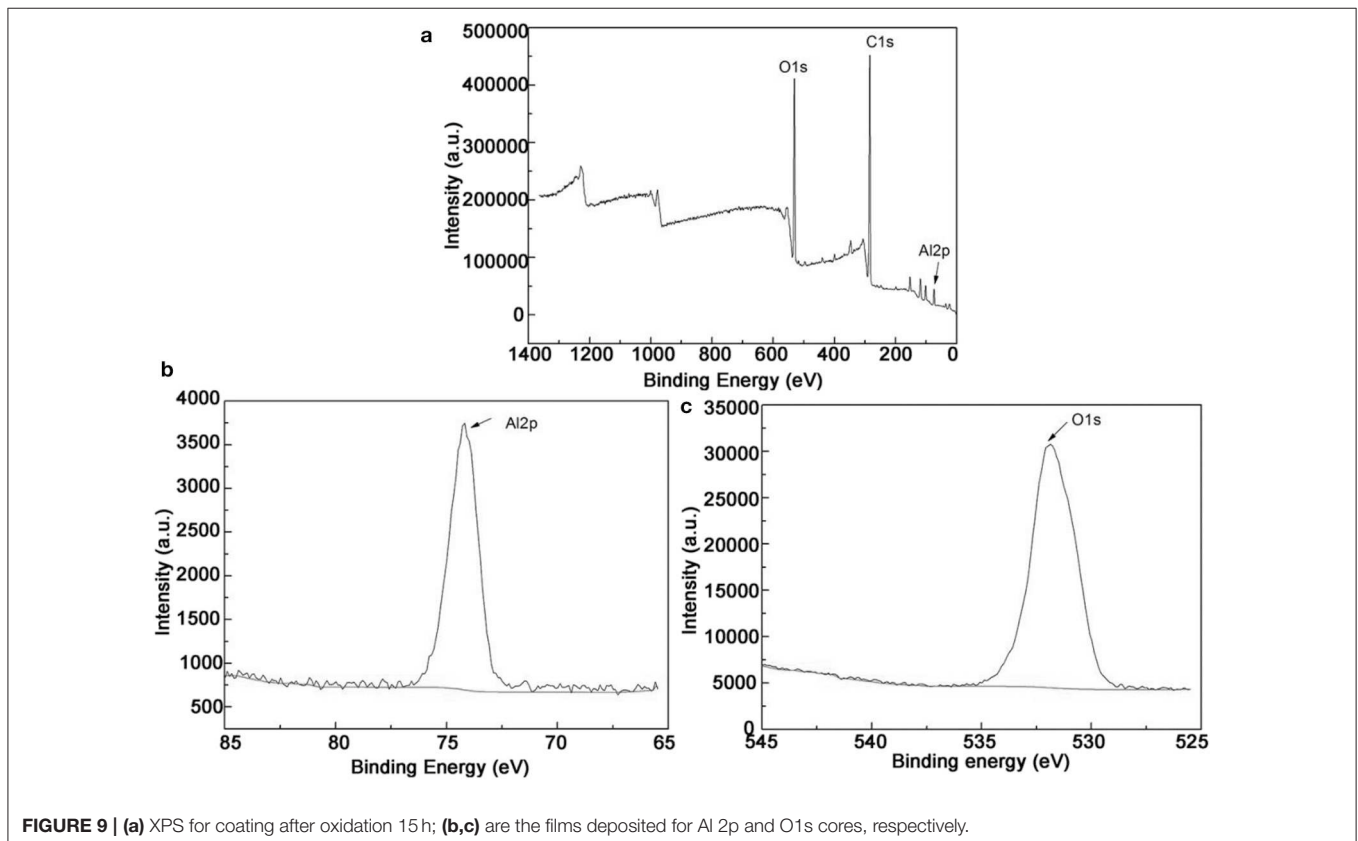
Oxide Scale Phase Constituents and Morphologies

Phase analysis of S1 and S4 samples after oxidation was carried out by XRD. **Figure 8** shows XRD patterns of samples S1 after



different oxidation time. It can be seen that Al_4W phase is detected on all the coating samples with different oxidation time. The Al_4W was still present even after 15 oxidation treatments with weaker diffraction intensity compared to the samples treated by 5- and 10-h oxidation. The initial aluminide coating was melted during oxidation process. Therefore, a reaction occurred between Al and W during the packing cementation, and an intermetallic compound with a high melting point was generated. During the high-temperature oxidation process, Al in the coating formed by the packing cementation triggered the growth of a protective oxide layer with high adhesion. This intermetallic phase was reported as oxidation-resistant (Ulrich and Galetz, 2016). After 15 h of oxidation, weak diffraction peaks of WO_3 phase were present in the XRD pattern, indicating weakened oxidation resistance compared with the first 10 h of oxidation, mainly due to local spallation on sample edges, which is consistent with the results of a previous study (Zou et al., 2013; Schmitt et al., 2014; Bakhtiary-Noodeh et al., 2017). Although diffraction peaks of Al_2O_3 are not observed in XRD, Al and O elements were detected in the sample by XPS, as shown in **Figure 9**, in which the Al 2p and O 1s peaks are inspected at 74.2 and 531.8 eV, respectively, similar to those of Al_2O_3 (Iatsunskyi et al., 2015; Xu et al., 2016). Therefore, it indicates that Al_2O_3 was generated on the surface during oxidation. All binding energies are referenced to the C1s hydrocarbon peak at 296 eV.

Figure 10 shows the surface morphology and 3D profile of sample S1 after 10 and 15 h of oxidation. As shown in **Figure 10A**,



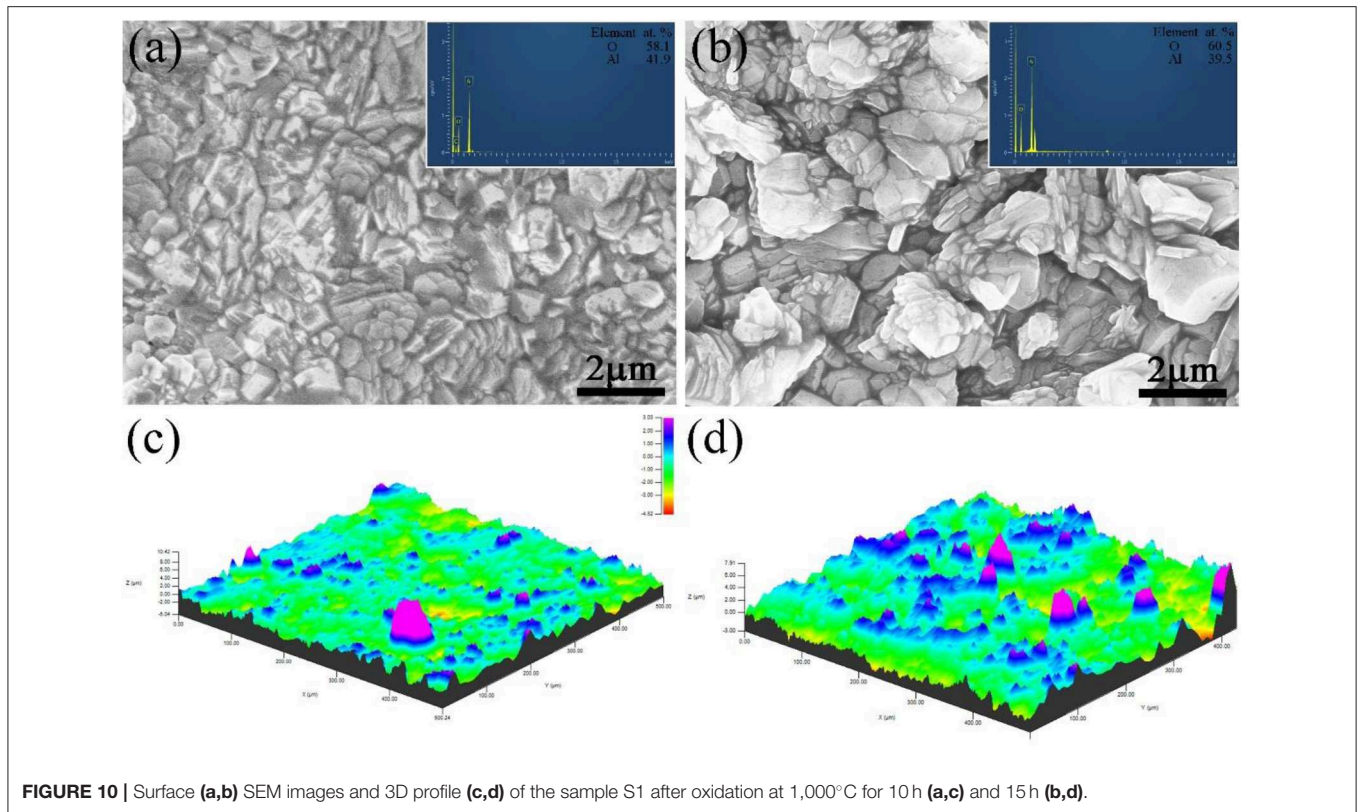


FIGURE 10 | Surface (a,b) SEM images and 3D profile (c,d) of the sample S1 after oxidation at 1,000°C for 10 h (a,c) and 15 h (b,d).

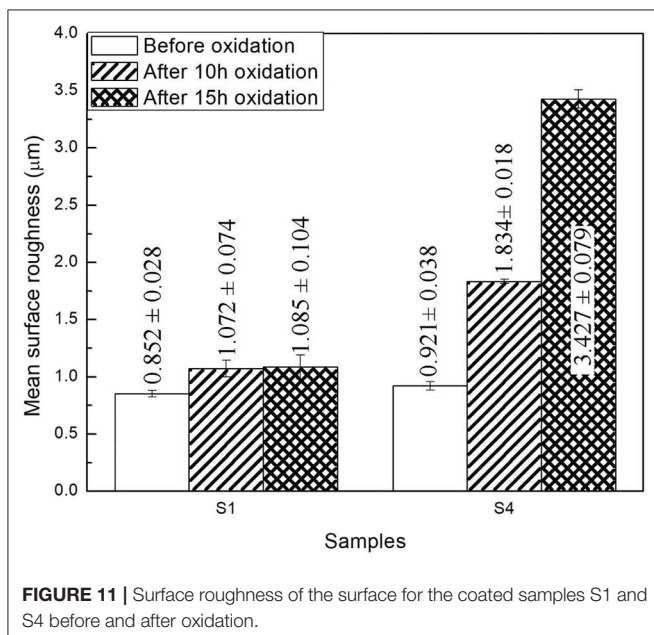


FIGURE 11 | Surface roughness of the surface for the coated samples S1 and S4 before and after oxidation.

a dense and continuous layer was produced after oxidation at 1,000°C for 10 h, and a large amount of gray scales were densely distributed on the surface. Composition of the surface was determined by EDS as shown in the top-right corner of Figure 10, displaying 60.5 O–39.5 Al (at. %) on the surface. The atomic

ratio of O element to Al is ~ 1.5 conforming to the stoichiometry of Al_2O_3 , which is consistent with the XPS pattern in Figure 9. However, a relatively loose surface microstructure with holes was formed after oxidation at 1,000°C for 15 h, as shown in Figure 10B. Obviously, grain size of the coating became larger by prolonging the oxidation time from 10 to 15 h. Figure 10 shows a 3D profile of the coated samples after 10 and 15 h of cyclic oxidation, and the surface roughness values are presented in Figure 11. The 10- and 15-h-oxidation specimens of S1 exhibit similar roughness with values of 1.072 ± 0.074 and $1.085 \pm 0.104 \mu\text{m}$, respectively, as shown in Figure 11. No obvious changes are discerned on the roughness of the coating, which could be attributed to superior stability of the microstructure and compactness (Kupkam et al., 2016). X-ray diffractometer results shown in Figure 12 illustrate diffraction peaks corresponding to sample S4 after oxidation for 5, 10, and 15 h, respectively. X-ray diffractometer analysis confirms that the surface of the constituent scale is mainly SiO_2 .

Figure 13 shows surface and cross-sectional morphologies of the silicide specimen S4 after cyclic oxidation at 1,000°C for 10 and 15 h, respectively. As shown in Figure 13A, the coating exhibits dense and uniform fine-grained surface after cyclic oxidation at 1,000°C for 10 h. Composition of the coated sample after cyclic oxidation for 10 and 15 h is shown in the top-right corner of Figure 13, and the surface contains 67.3 O–32.7 Si (at. %) implying the formation of SiO_2 . After oxidation at 1,000°C for 15 h, as shown in Figure 13B, the surface morphology of the Al-Si coating shows some visible pores and a relatively

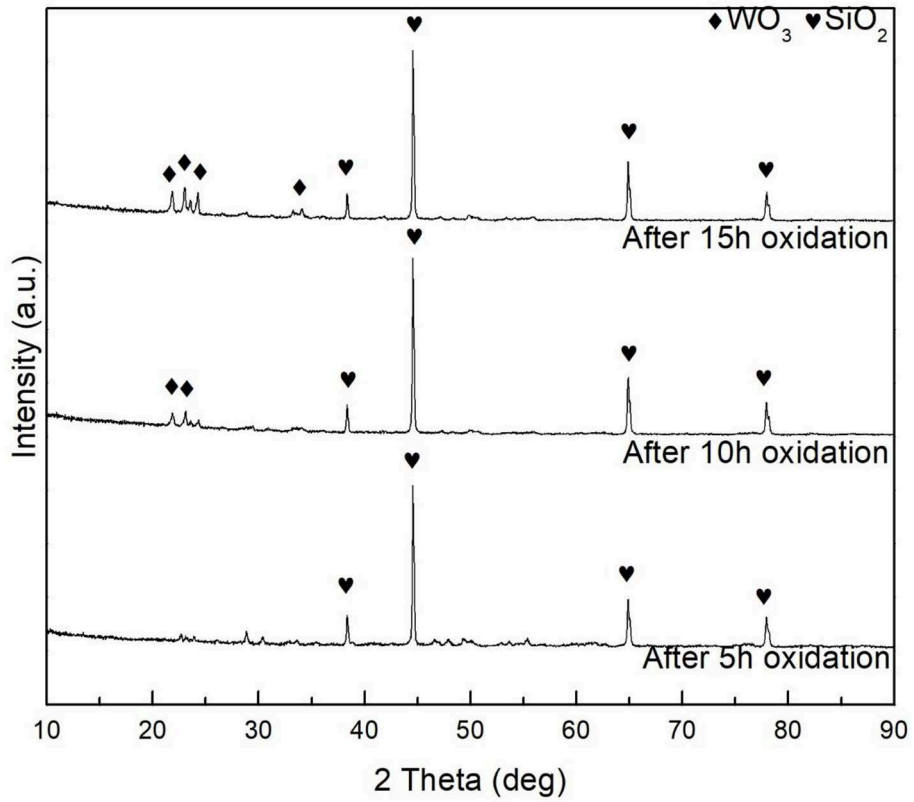


FIGURE 12 | X-ray diffractometer patterns of the samples S4 after cyclic oxidation test.

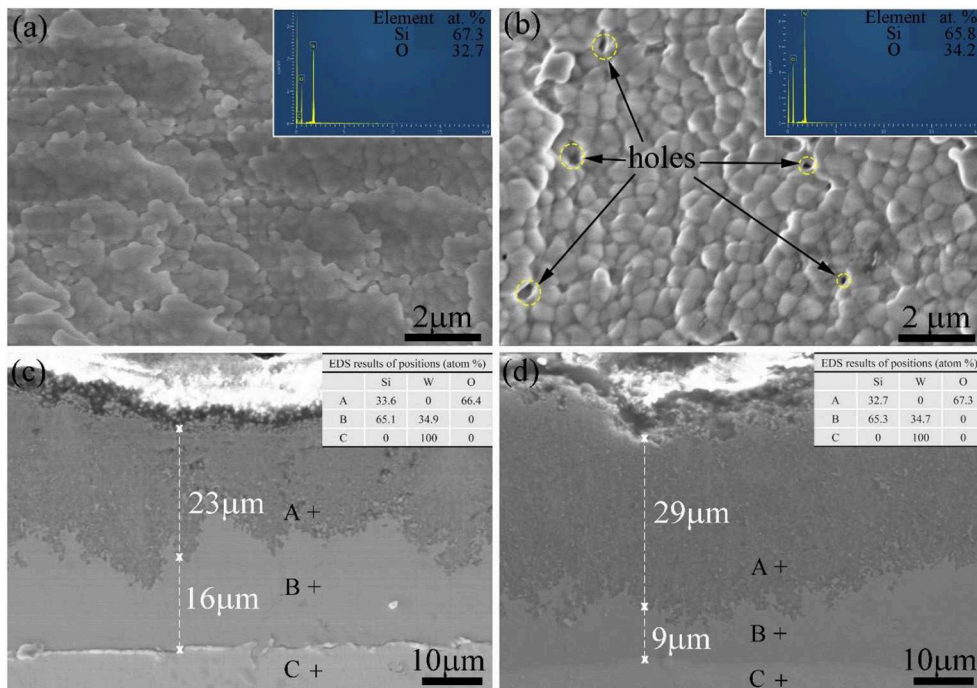


FIGURE 13 | Surface (a,b) and cross-sectional (c,d) SEM images of the sample S4 after oxidation at 1,000°C for 10h (a,c) and 15h (b,d).

smoother surface compared with that after 10-h oxidation. This finding matches well with the previous studies (Pourasad and Ehsani, 2017; Liu Y. et al., 2018). **Figure 13C** shows cross-section morphology image of the coating sample S4 after oxidation at 1,000°C for 10 h. It can be observed that the layer is dense and uniform with the thickness of $\sim 22.5 \mu\text{m}$. Under the scale, there is a 22.5- μm -thick residual coating. Energy-dispersive X-ray spectroscopy analysis reveals that the layer is mainly composed of WSi_2 . **Figure 13D** shows morphology of cross section after cyclic oxidation at 1,000°C for 15 h. It can be seen from **Figure 13D** that a continuous and dense antioxidation coating with a thickness of $\sim 29 \mu\text{m}$ was formed on the surface after the coating sample S4 was oxidized for 15 h. Energy-dispersive X-ray spectroscopy and XRD characterization confirms that the phase of the scale is also mainly composed of SiO_2 . And after the cyclic oxidation, a dense and uniform WSi_2 layer still exists under the SiO_2 layer. Therefore, it is reasonable to assume that the Si element in the coating during oxidation process first forms an SiO_2 coating in a high-temperature oxidation environment, thereby blocking oxygen from further penetration into the substrate. Under the SiO_2 layer, a 16- μm -thick coating is observed, and EDS analysis suggests that the layer is mainly WSi_2 . As exhibited in **Figure 11**, the surface roughness value of specimen S4 is 1.834 ± 0.018 and $3.427 \pm 0.079 \mu\text{m}$, respectively, after oxidation for 10 and 15 h. Lower roughness was obtained on the sample S1 after oxidation for 10 h than that for 15 h, owing to more compact and flatter surface (Wang C. et al., 2018). Comparing to **Figures 13C,D**, it can be observed that oxygen reacted with aluminized layer and siliconized layer to form dense and uniform aluminum oxide and silicon oxide layers with increasing oxidation time, thereby improving the oxidation performance of the samples.

REFERENCES

- Bakhtyari-Noodeh, M., Moradian, S., and Ranjbar, Z. (2017). Edge protection improvement of automotive electrocoating in the presence of silica nanoparticles. *Surf. Coat. Technol.* 317, 134–147. doi: 10.1016/j.surfcoat.2017.03.004
- Bobzin, K., Brogelmann, T., Kalscheuer, C., and Liang, T. (2018). Al-Si and Al-Si-Y coatings deposited by HS-PVD for the oxidation protection of γ -TiAl. *Surf. Coat. Technol.* 350, 587–595. doi: 10.1016/j.surfcoat.2018.06.074
- Bozza, F., Bolelli, G., Giolli, C., Giorgetti, A., Lusvarghi, L., Sassatelli, P., et al. (2014). Diffusion mechanisms and microstructure development in pack aluminizing of Ni-based alloys. *Surf. Coat. Technol.* 239, 147–159. doi: 10.1016/j.surfcoat.2013.11.034
- Cai, Z., Zhao, X., Zhang, D., Wu, Y., Wen, J., Tian, G., et al. (2018). Microstructure and oxidation resistance of a YSZ modified silicide coating for Ta-W alloy at 1800 °C. *Corros. Sci.* 143, 116–128. doi: 10.1016/j.corsci.2018.08.007
- Cheng, J. C., Yi, S. H., and Park, J. S. (2015). Simultaneous coating of Si and B on Nb-Si-B alloys by a halide activated pack cementation method and oxidation behaviors of the alloys with coatings at 1100 °C. *J. Alloy Compd.* 644, 975–981. doi: 10.1016/j.jallcom.2015.05.003
- Ge, Y., Wang, Y., Chen, J., Zou, Y., Guo, L., Ouyang, J., et al. (2018). An Nb_2O_5 - SiO_2 - Al_2O_3 - NbSi_2 / Nb_5Si_3 multilayer coating on Nb-Hf alloy to improve oxidation resistance. *J. Alloy Compd.* 745, 271–281. doi: 10.1016/j.jallcom.2018.02.107
- Iatsunskyi, I., Kempinski, M., Jancelewicz, M., Zaleski, K., Jurga, S., Smytynna, V., et al. (2015). Structural and XPS characterization of ALD Al_2O_3 coated porous silicon. *Vacuum* 113, 52–58. doi: 10.1016/j.vacuum.2014.12.015

SUMMARY AND CONCLUSION

A dense and uniform aluminide and silicide coating was obtained through high-activity pack cementation at 1,000°C for 5 h. Cyclic oxidation tests were performed on each sample at 1,000°C, and changes in the microstructure of the coating before and after oxidation were investigated. The conclusions are as follows:

- (1) An interface layer consisting of WSi_2 and Al_4W was observed for the pure tungsten because of the interdiffusion of Si, Al, and W during HAPC.
- (2) The aluminide and silicide coating prepared at 1,000°C for 5 h retained comparatively good cyclic oxidation resistance. After oxidation, a dense scale consisting of SiO_2 and Al_2O_3 formed on the coating. The oxidation rate of the coating was lower than that of the pure tungsten.
- (3) With increasing oxidation time, oxygen reacted with aluminized and siliconized layers to form dense and uniform aluminum oxide and silicon oxide layers, thereby improving the oxidation performance of the material.

DATA AVAILABILITY STATEMENT

The raw data supporting the conclusions of this article will be made available by the authors, without undue reservation, to any qualified researcher.

AUTHOR CONTRIBUTIONS

LZ and Y-XZ conducted the experiment and drafted the manuscript. L-ML supervised the experiments. LZ, L-ML, and J-FW were involved in the data analysis and discussions.

- Kupkam, M., Marut, J., Aniolek, K., and Barylski, A. (2016). The effect of oxide scale roughness on the plasticity of iron aluminide alloy. *Vacuum* 132, 111–118. doi: 10.1016/j.vacuum.2016.07.034
- Liu, D. G., Zheng, L., Luo, L. M., Zan, X., Song, J. P., Xu, Q., et al. (2018). An overview of oxidation-resistant tungsten alloys for nuclear fusion. *J. Alloy Compd.* 765, 299–312. doi: 10.1016/j.jallcom.2018.06.202
- Liu, Y., Shao, W., Wang, C., and Zhou, C. (2018). Micro structure and oxidation behavior of Mo-Si-Al coating on Nb-based alloy. *J. Alloy Compd.* 735, 2247–2245. doi: 10.1016/j.jallcom.2017.11.339
- Majumdar, S., Paul, B., Kain, V., and Dey, G. K. (2017). Formation of Al_2O_3 / Fe-Al layers on SS 316 surface by pack aluminizing and heat treatment. *Mater. Chem. Phys.* 190, 31–37. doi: 10.1016/j.matchemphys.2017.01.002
- M'Saoubi, R., Alm, O., Andersson, J. M., Engström, H., Larsson, T., Johansson-Jøesaar, M. P., et al. (2017). Microstructure and wear mechanisms of texture-controlled CVD α - Al_2O_3 coatings. *Wear* 376, 1766–1778. doi: 10.1016/j.wear.2017.01.071
- Oukati, S. F., Sharifitabar, M., and Shaflee Afarani, M. (2018). Synthesis of Ti-Si-Al coatings on the surface of Ti-6Al-4V alloy via hot dip siliconizing route. *Surf. Coat. Technol.* 337, 349–356. doi: 10.1016/j.surfcoat.2018.01.037
- Pei, H., Wen, Z., Zhang, Y., and Yue, Z. (2017). Oxidation behavior and mechanism of a Ni-based single crystal superalloy with single α - Al_2O_3 film at 1000°C. *Appl. Surf. Sci.* 411, 124–135. doi: 10.1016/j.apsusc.2017.03.116
- Portebois, L., Mathieu, S., Bouizi, Y., and Vilasi, M. (2014). Effect of boron addition on the oxidation resistance of silicide protective coatings: a focus on boron location in as-coated and oxidized coated niobium alloys. *Surf. Coat. Technol.* 253, 292–299. doi: 10.1016/j.surfcoat.2014.05.058

- Pourasad, J., and Ehsani, N. (2017). *In-situ* synthesis of SiC-ZrB₂ coating by a novel pack cementation technique to protect graphite against oxidation. *J. Alloy Compd.* 690, 692–698. doi: 10.1016/j.jallcom.2016.08.112
- Pulci, G., Tirillò, J., Marra, F., Sarasini, F., Bellucci, A., Valente, T., et al. (2015). High temperature oxidation of MCrAlY coatings modified by Al₂O₃ PVD overlay. *Surf. Coat. Technol.* 268, 198–204. doi: 10.1016/j.surfcoat.2014.09.048
- Qiao, M., and Zhou, C. (2013). Codeposition of Co-Al-Y on nickel base superalloys by pack cementation process. *Corros. Sci.* 79, 454–460. doi: 10.1016/j.corsci.2013.06.033
- Qiao, Y. Q., Kong, J. P., and Guo, X. P. (2018). Hot corrosion phenomena of Nb-Ti-Si based alloy and its silicide coating induced by different corrosive environments at 900 °C. *Ceram. Int.* 44, 7978–7990. doi: 10.1016/j.ceramint.2018.01.238
- Schmitt, M., Scharfer, P., and Schabel, W. (2014). Slot die coating of lithium-ion battery electrodes: investigations on edge effect issues for stripe and pattern coatings. *J. Coat. Technol. Res.* 11, 57–63. doi: 10.1007/s11998-013-9498-y
- Sun, J., Fu, Q., and Guo, L. (2016). Influence of siliconizing on the oxidation behavior of plasma sprayed MoSi₂ coating for niobium based alloy. *Intermetallics* 72, 9–16. doi: 10.1016/j.intermet.2016.01.006
- Sun, Y., Dong, J., Zhao, P., and Dou, B. (2017). Formation and phase transformation of aluminide coating prepared by low temperature aluminizing process. *Surf. Coat. Technol.* 330, 234–240. doi: 10.1016/j.surfcoat.2017.10.025
- Swadzba, R. (2018). Interfacial phenomena and evolution of modified aluminide bondcoatings in thermal barrier coatings. *Appl. Surf. Sci.* 445, 133–144. doi: 10.1016/j.apsusc.2018.03.137
- Tan, X. Y., Klein, F., Litnovsky, A., Wegener, T., Schmitz, J., Linsmeier, C. H., et al. (2019). Evaluation of the high temperature oxidation of W-Cr-Zr self-passivating alloys. *Corros. Sci.* 147, 201–211. doi: 10.1016/j.corsci.2018.11.022
- Tian, X., Guo, X., Sun, Z., Yin, Z., and Wang, L. (2014). Formation of B-modified MoSi₂ coating on pure Mo prepared through HAPC process. *Int. J. Refract. Met. Hard Mater.* 45, 8–14. doi: 10.1016/j.ijrmhm.2014.03.003
- Ulrich, A. S., and Galetz, M. C. (2016). Protective aluminide coating for refractory metals. *Oxid Met.* 86, 511–535. doi: 10.1007/s11085-016-9650-z
- Wang, C. C., Li, K. Z., He, Q. C., Huo, C., and Shi, X. (2018). Oxidation and ablation resistant properties of pack-siliconized Si-C protective coating for carbon/carbon composites. *J. Alloy Compd.* 741, 937–950. doi: 10.1016/j.jallcom.2018.01.214
- Wang, L., Fu, Q., Zhao, F., and Zhao, Z. (2018). Constructing self-healing ZrSi₂-MoSi₂ coating for C/C composites with enhanced oxidation protective ability. *Surf. Coat. Technol.* 347, 257–269. doi: 10.1016/j.surfcoat.2018.05.002
- Wang, S. M., Sun, C. X., Guo, W. H., Yan, Q., Zhou, Z., Zhang, Y., et al. (2014). Review on the explosive consolidation methods to fabricate tungsten-based PFMs. *J. Nucl. Mater.* 455, 174–179. doi: 10.1016/j.jnucmat.2014.05.073
- Wang, Y., Guo, X. P., and Qiao, Y. Q. (2017). Interactions between Nb-Si based ultrahigh temperature alloy and yttria matrix mould shells. *Mater. Des.* 116, 461–471. doi: 10.1016/j.matdes.2016.12.033
- Wu, L. K., Wu, J. J., Wu, W. Y., Hou, G. Y., Cao, H. Z., Tang, Y. P., et al. (2019). High temperature oxidation resistance of γ -TiAl alloy with pack aluminizing and electrodeposited SiO₂ composite coating. *Corr. Sci.* 146, 18–27. doi: 10.1016/j.corsci.2018.10.031
- Wu, L. K., Wu, W. Y., Song, J. L., Hou, G. Y., Cao, H. Z., Tang, Y. P., et al. (2018). Enhanced high temperature oxidation resistance for γ -TiAl alloy with electrodeposited SiO₂ film. *Corr. Sci.* 140, 388–401. doi: 10.1016/j.corsci.2018.05.025
- Xu, Y. P., Zhao, S. X., Liu, F., Li, X. C., Zhao, M. Z., Wang, J., et al. (2016). Studies on oxidation and deuterium permeation behavior of a low temperature α -Al₂O₃ forming Fe-Cr-Al ferritic steel. *J. Nucl. Sci. Technol.* 477, 257–262. doi: 10.1016/j.jnucmat.2016.04.054
- Zhang, J., Fan, Y., Zhao, X., Ma, R., Du, A., and Cao, X. (2018). Influence of duty cycle on the growth behavior and wear resistance of micro-arc oxidation coatings on hot dip aluminized cast iron. *Surf. Coat. Technol.* 337, 141–149. doi: 10.1016/j.surfcoat.2017.12.064
- Zou, X., Fu, Q. G., Liu, L., Li, H., Wang, Y., Yao, X., et al. (2013). ZrB₂-SiC coating to protect carbon/carbon composites against ablation. *Surf. Coat. Technol.* 226, 17–21. doi: 10.1016/j.surfcoat.2013.03.027

Conflict of Interest: The authors declare that the research was conducted in the absence of any commercial or financial relationships that could be construed as a potential conflict of interest.

Copyright © 2020 Zhu, Zhang, Wang and Luo. This is an open-access article distributed under the terms of the Creative Commons Attribution License (CC BY). The use, distribution or reproduction in other forums is permitted, provided the original author(s) and the copyright owner(s) are credited and that the original publication in this journal is cited, in accordance with accepted academic practice. No use, distribution or reproduction is permitted which does not comply with these terms.